Global Nonlinear Simulations of Ion and Electron Turbulence Usintg a Particle-In-Cell Approach

S. Jolliet 1), B. F. McMillan 1), T. M. Tran 1), X. Lapillonne 1), L. Villard 1), A. Bottino 2), P. Angelino 3)

1) Association Euratom-Confédération Suisse, EPFL/SB/CRPP, Station 13, CH-1015, Lausanne, Switzerland

2) Max Planck Institut für Plasmaphysik, IPP-EURATOM Association, Garching, Germany

3) DRFC, Association EURATOM, CEA Cadarache, 19018 Saint-Paul-Lez-Durance, France

e-mail contact of main author: sebastien.jolliet@epfl.ch

Abstract

Ion-Temperature-Gradient and Trapped-Electron-Mode are two most likely candidates to explain the anomalous transport observed in Tokamaks. These turbulent phenomena are studied with the help of the gyrokinetic theory. These simulations require huge CPU power. The different numerical schemes all have some serious limitations. In the case of the Particle-in-Cell approach, the unavoidable statistical noise prevents the simulations to be run for long times. In this work, the global gyrokinetic PIC code ORB5 is applied to study three different issues related to gyrokinetics. First, it is shown by direct simulations that a steady state can be reached if a small, artificial dissipative term is added to the Vlasov equation. Second, it is shown that the parallel nonlinearity term in the parallel velocity equation of motion has very little influence on the zonal flow structures and on the heat transport provided the signal to noise ratio of the simulation is sufficiently high. Third, preliminary long and statistically converged global TEM simulations are presented. Basic features of TEM turbulence are presented and the role of the zonal flow is examined.

1. Introduction

Understanding turbulence driven by micro-instabilities such as Ion Temperature Gradient (ITG) or Trapped Electron Modes (TEM) is one of the key issues to accurately predict the performance of future Tokamak devices such as ITER. Particle-In-Cell (PIC) method is a very efficient tool to study turbulence in plamas. Unfortunately, it suffers from statistical noise, which makes it impossible to perform long simulations (up to transport time scales). Numerical noise has been proposed [1] as one of the candidate to explain the discrepancies observed for ETG simulations [2,3]. For ITG turbulence, many algorithms have been developed to reduce numerical noise but its impact on the results is rarely discussed. In fact, the main limitation of collisionless PIC simulations is that they cannot achieve a steady steate but only a quasi-steady state [4] where the sum of the square weights continuously grows. The solution is to introduce dissipation, which can be done by implementing collisions. However, this a difficult task in PIC codes due to the weight spreading phenomena [5]. Instead, Krommes [4] proposed to introduce dissipation with a W-stat. A noise-control operator (NCO) based on this idea has been implemented in [6] in the global collisionless gyrokinetic PIC code ORB5 [7]. It allows running statistically long, converged simulations with high signal to noise ratios (SNR).

In this work, the new version of the code has been used to explore three important issues of gyrokinetic micro turbulence. The first one is the establishment of a steady state as described

above. The second one is the role of the v-parallel nonlinearity (VNL). It is found by some PIC codes [8,9,10,11] that this term in the equations of motion modifies the zonal flow structure for both and cylinder and tokamak geometry, while some Eulerian [12] and PIC [13] codes have not observed a significant role. Finally, the third topic of this work addresses nonlinear global TEM turbulence, which is much more difficult to simulate than the ITG case because the ion and the fast electron time scales must be simultaneously resolved. Local flux-tube simulations [14,15] are still controversial for the role of the zonal flow.

This paper is organized as follows. Section 2 gives a brief presentation of the ORB5 code, with an emphasis on the NCO. In section 3, the entropy diagnostic is derived and the final states of ITG simulations are studied. Section 4 shows the influence of the VNL on both decaying and driven ITG simulations. In section 5, preliminary global nonlinear TEM simulations are presented, and the role of the zonal flow is examined. Finally, conclusions are exposed in Section 6.

2. The global PIC code ORB5

All the simulations presented in this paper are collisionless and electrostatic. The ORB5 code solves Hahm's gyrokinetic equations [16] in Tokamak geometry, The distribution function f is split into a Maxwellian part f_0 and a perturbed part δf. Note that ORB5 is not a δf code. This decomposition can be viewed as a control variates method [17]. The equations of motion of the space coordinates contain the parallel motion, the curvature, ∇B and diamagnetic linear drifts as well as the nonlinear ExB drift. The magnetic moment is conserved, and the equation of motion for the parallel velocity $v_{//}$ is given by:

$$\frac{dv_{\parallel}}{dt} = \frac{1}{2}v_{\perp}^2 \nabla \cdot \vec{h} + \frac{v_{\perp}^2 v_{\parallel}}{2B_{\parallel}^* \Omega_i B} \left\{ \vec{h} \times \left[\vec{h} \times (\nabla \times B) \right] \right\} \cdot \nabla B$$

$$+ \langle \vec{E} \rangle \cdot \left\{ \frac{q_i}{m_i}\vec{h} + \frac{v_{\parallel}}{BB_{\parallel}^*} \left(\vec{h} \times \nabla B \right) - \frac{v_{\parallel}}{BB_{\parallel}^*} \left\{ \vec{h} \times \left[\vec{h} \times (\nabla \times B) \right] \right\} \right\} \quad (1)$$

$$\Omega_i = \frac{q_i B}{m_i}, \vec{h} = \frac{\vec{B}}{B}, B_{\parallel}^* = \vec{B} \cdot \vec{h} + \frac{m_i v_{\parallel}}{q_i} \left(\nabla \times \vec{h} \right) \cdot \vec{h}$$

q_i and m_i are the ion charge and mass and B is the magnetic field, and "$< >$" denotes the gyroaverage. The first term is the mirror term, the second term is an interaction tem between the pressure and magnetic field gradient and the third term is the VNL. The Vlasov equation is:

$$\frac{d\delta f}{dt} = -\frac{\partial f_0}{\partial \Psi}\frac{d\Psi}{dt} - \frac{\partial f_0}{\partial \epsilon}\frac{d\epsilon}{dt} - \gamma_K \delta f + \sum_{i=1}^{N} g_i(s,t)f_0 M_i \quad (2)$$

The Maxwellian used is a canonical Maxwellian with a correction described with the unperturbed constant of motion Ψ to avoid spurious zonal flows [18], and ε is the kinetic energy. The first term, containing the equilibrium gradient, is the driving term. The second term describes the energy transfer from the particles to the perturbation. The third and fourth term compose the NCO. γ_K is the Krook damping, and the fourth term is a correction term, applied on each magnetic surface s, such that the damping term conserves N specified moments M. $\{g_i\}$ are unknowns computed at each time step. The conserved moments M are the density, the energy and a zonal flow preserving moment (see [6]). If the NCO does not conserve the energy, it will restore the distribution function towards a Maxwellian and will

act as a heating. If it conserves the energy the gradients will relax. A more complete description of the NCO can be found in [6].

The system is closed with the quasi-neutrality equation:

$$[1 - \bar{\alpha}_b(\psi)] \frac{en_0(\psi)}{T_e(\psi)} [\phi(\vec{x}, t) - \bar{\phi}(\psi, t)] - \nabla_\perp \cdot \left[\frac{n_0(\psi)}{B\Omega_i} \nabla_\perp \phi(\vec{x}, t) \right] = \delta n_i(\vec{x}, t) - \frac{1}{Z_i} \delta n_e(\vec{x}, t)$$

(3)

In this model, the trapped electrons are drift kinetic (with fraction α_b) and the passing electrons are adiabatic. The first term is the adiabatic term, the second term is the polarization density written in the long wavelength limit and the RHS is the perturbed density. The adiabatic case is obtained by setting $\alpha_b = \delta n_e = 0$. Trapped electrons can be nonlinearly detrapped and will not be taken into account in the charge assignment. In a very small region near the edge, the equilibrium density appearing in the quasi-neutrality equation is multiplied by a shielding term to avoid spurious generation of zonal flow at the plasma edge. This equation is solved with cubic B-splines finite elements [19] using the straight-field line coordinate. It is solved in toroidal and poloidal Fourier space and is Fourier filtered: it retains only the field-aligned mode $m=nq(s)+\Delta m$ where Δm is an input parameter ($\Delta m=5$ will be used in this paper). More details on the numerization of ORB5 can be found in [7]. The code has been successfully benchmarked for a selection of linear and nonlinear tests [7].

3. The fluctuation entropy diagnostic

The evolution of the fluctuation entropy, defined according to [13], is obtained by multiplying the Vlasov equation, Eq. (2), by $\delta f / f_0$ and integrating over phase space:

$$\begin{aligned}
\frac{d\delta S}{dt} &= \frac{1}{2}\frac{d}{dt} \int \frac{\delta f^2}{f_0} d\vec{z} = D_{\text{flux}} + D_{\text{field}} + D_{\text{nc}} \\
D_{\text{flux}} &= -\int \left(\frac{\delta f}{f_0} + \frac{\delta f^2}{2f_0^2} \right) \frac{\partial f_0}{\partial \Psi} \frac{d\Psi}{dt} d\vec{z} \\
D_{\text{field}} &= -\int \left(\frac{\delta f}{f_0} + \frac{\delta f^2}{2f_0^2} \right) \frac{\partial f_0}{\partial \epsilon} \frac{d\epsilon}{dt} d\vec{z} \\
D_{\text{nc}} &= -\int \gamma_K \frac{\delta f^2}{f_0} + \sum_{i=1}^{N} g_i(s,t) \delta f M_i d\vec{z}
\end{aligned}$$

(4)

It is instructive to note that in the local limit with constant gradients, and second order terms (in δf^2) neglected, D_{flux} obtained from the driving term of the Vlasov equation is proportional to the heat diffusivity χ [20] and D_{field} is proportional to dW/dt where W is the total perturbed field energy of the system. D_{nc} is the dissipative term due to the NCO. When this term is absent the system can only evolve towards a quasi-steady state characterized by $D_{field}=0$ and a constant D_{flux} (~the heat diffusivity) balancing the entropy production: the sum of the square weights will grow, leading to a noise-dominated situation. In order to test the effects of the NCO on the entropy productions, nonlinear CYCLONE [21] simulations have been performed at $\rho^*=\rho_s/a=1/184$ where ρ_s is the ion sound gyroradius and a the minor radius, $R_0/L_T=6.9$, $T_e=T_i$, $s=0.78$, $\eta_i=3.12$, $r_0=0.5$, $q(\rho_0)=1.4$, $B_0=1.91$ and $a/R_0=0.18$. The quasineutrality equation is solved on a $N_s x N_\chi x N_\varphi=128 x 512 x 256$ grid with 80M markers, corresponding to 5 particles/cell but 220 particles per Fourier mode, which is the meaningful ratio [22]. The Krook damping term is $\gamma_K=9\cdot10^{-5}\Omega^{-1}$ which is one tenth of the maximal linear
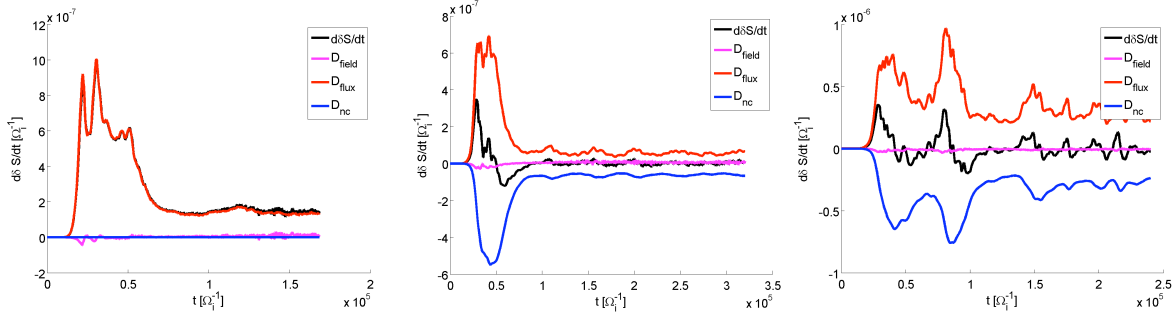
FIGURE 1. *time evolution of the fluctuation entropy production rate, D_{flux}, D_{field} and D_{nc} for a transient (left), noise-controlled (middle) and heated simulation (right)*

growth rate. Three different simulations have been performed. A t*ransient* simulation where the NCO is switched off, a *noise-controlled simulation* where the NCO is switched on and conserves the energy, leading to profile relaxation and a *heated* simulation where the NCO does not conserve the energy and acts like a heating.

Fig.1 shows the time evolution of δS and the different components of the fluctuation entropy balance equation. The transient simulation clearly exhibits a quasi-steady state. In the end of the simulation, the entropy production is balanced by D_{flux} while D_{field} is close to 0. This is the situation with saturated low-order moments and growing entropy. This simulation therefore becomes rapidly dominated by numerical noise: the SNR is equal to 1 in the end of the simulation. Note that the signal (resp. the noise) is obtained by summing the components of the perturbed density in poloidal and toroidal Fourier space inside (resp. in a diagonal band outside) the Fourier field-aligned filter. On the other hand, the noise-controlled simulation exhibits a steady state. The dissipative term D_{nc} is always negative, balances D_{flux} (note that the bursts of D_{nc} are slightly shifted in time with those of D_{flux}). Like for the transient case D_{field} is close to 0. This simulation has constant entropy in the late nonlinear phase. This proves that a W-stat allows a steady state. However, the SNR is round 6 at the end of the simulation, meaning that the late-time fluxes are questionable. The NCO greatly improves the SNR but the difficulty to approach the critical gradient still remains. In the heated simulation, the fluctuation entropy evolution is more bursty due to the higher turbulent activity, but $d\delta S/dt$ is on average very close to 0. It means that driven simulations with a NCO operator reach a steady state. In this case the SNR is oscillating around a constant value of 25, meaning that the simulation could be run up to arbitrarily long times.

4. The influence of the parallel nonlinearity

Including the VNL means retaining the third term of Eq. (1) in the equation of motion. From the physical point of view, this term produces nonlinear Landau damping. Its role is still controversial. It is of order $O(\varepsilon_g^2)$, where ε_g is the small parameter used in the gyrokinetic ordering [16] and should therefore be small. However, global PIC simulations performed with the global PIC codes GTC [8], UCAN [9] and ORB5 [11] showed an influence of the VNL (although it is "strongly diminished" at $\rho^*=1/180$ for the UCAN code), whereas simulations performed with the flux tube GEM and the Eulerian code GYRO [12] did not reveal any significant role of this term. All these simulations had very few particles per cell. In the case of ORB5, the field-aligned Fourier filter was not implemented but an optimized loading technique was used [23]. Unfortunately no SNR diagnostic was available. Now that many improvements have been done on ORB5, the role of the VNL is revisited. The CYCLONE
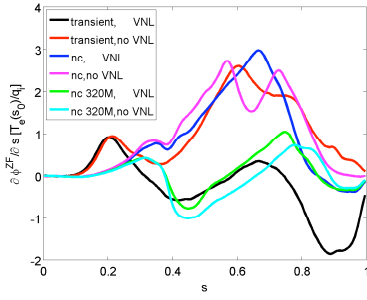
FIG. 2. radial structure of the radial electric field, averaged between t=541 (10^5) and t=812 (1.5·10^5) [a/c_s] (Ω^{i-1}) for 80M markers transient and noise-controlled and 320M markers noise controlled simulations, with and without the VNL.
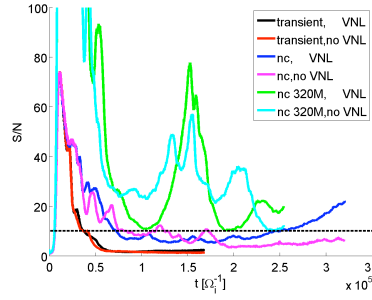
FIG. 3. Time evolution of the signal to noise ratio for 80M markers transient and noise-controlled and 320M markers noise-controlled simulations, with and without the VNL. The horizontal dashed line indicates a signal to noise ratio of 10
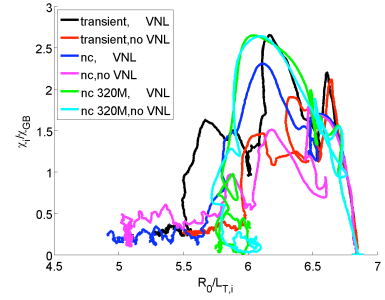
FIG. 4. χ_i/χ_{GB} vs R_0/L_T for 80M markers transient and noise-controlled and 320M markers noise-controlled simulations, with and without the VNL.

transient, noise-controlled and heated simulations have been run without the VNL. Fig. 2 shows the radial structure of the radial electric field, averaged between $t=541$ and $t=812$ [a/c_s] for 80M markers transient and noise-controlled simulation as well as 320M markers noise-controlled simulations. In the transient case, these structures are completely different. However, these simulations are completely noise-dominated in the time window considered, as the SNR are around 1. In the 80M markers noise-controlled case, these profiles are much more similar, although the case without the VNL has two peaks. The SNR are around 8 and so the results are still questionable. In the end of these simulations, the SNR go up: this is due to a spurious increase of the zonal flow near the edge and is the sign of noise-dominated simulations. This is why two noise-controlled simulations have been run with 320M markers, yielding much higher SNR. In this case the profiles of the radial electric field are even more similar.

The effect of the VNL on transport is examined on Fig. 4, which plots the heat diffusivity χ_i normalized to its Gyrobohm value $\chi_{GB}=\rho_s^2 c_s/a$ vs the normalized temperature gradient R_0/L_T.. Both profiles are radially averaged between $\rho_0/a=0.4$ and $\rho_0=0.6$. In the late nonlinear phase, the transient simulations have constant heat diffusivity with a time-decreasing temperature gradient. This is because the entropy grows and creates finer and finer structures in velocity space. The same phenomenon happens for 80M markers simulations because the steady state is not good enough for this number of markers; the 320M case is much better. Note that the curves will start to go horizontally as they reach the critical gradient. Nevertheless, the 320M case shows that there is very little differences. ORB5 simulations therefore confirm the conclusions of Ref. [12]. But, in addition, these results show that the differences previously observed both on the zonal flow structure and the transport likely result from numerical noise.

Finally, the influence of the VNL on driven ITG simulations is examined. Fig. 5 shows the profiles of the radial electric field averaged between 10^5 and $1.5·10^5\Omega_i^{-1}$ for 80M markers heated simulations. These profiles are extremely similar considering the chaotic nature of turbulence. The heat diffusivity and the temperature gradient are displayed on Figs. 6 and 7. Due to the bursty character of these curves, a moving time-average over 400 a/c_s has been performed. The errors bars are 2σ where σ is the standard deviation of the moving time-average. However, a proper comparison would need to run these simulations over longer

times and with different initializations to assess if the differences observed are due to random fluctuations or to the VNL. However, these curves lie within the error bars for both the heat diffusivity and the temperature gradient which tends to confirm that the VNL does not have an important impact on the heat transport.
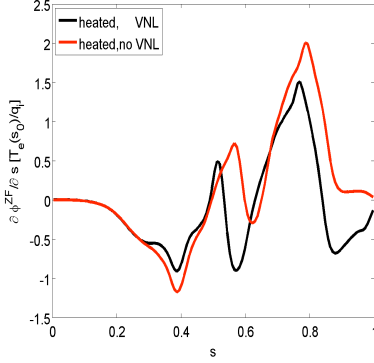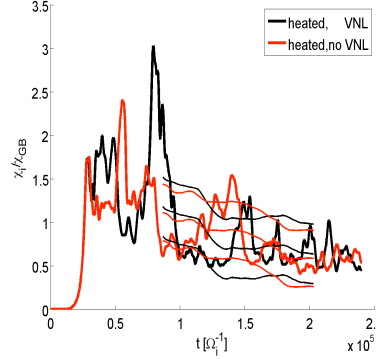

FIG.5. radial structure of the radial electric field, averaged between $t=541$ (10^5) and $t=812$ ($1.5 \cdot 10^5$) [a/c_s] (Ω^{i-1}) for 80M markers heated simulations

FIG. 6. Time evolution of χ_i/χ_{GB} for 80M markers heated simulations. The thin lines are the moving time-average (over 400 $a/cs \sim 8 \cdot 10 \Omega_i^{-1}$) $\pm 2\sigma$ where σ is the standard deviation of the moving time-average
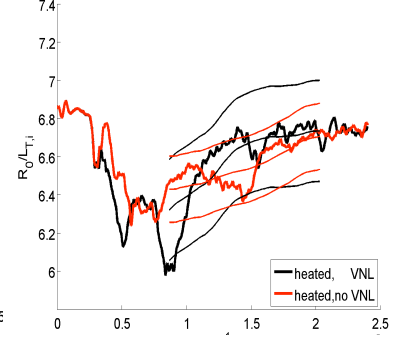
FIG. 7 Time evolution of R_0/L_T for 80M markers heated simulations. The thin lines are the moving time-average (over 400 $a/cs \sim 8 \cdot 10 \Omega_i^{-1}$) $\pm 2\sigma$ where σ is the standard deviation of the moving time-average

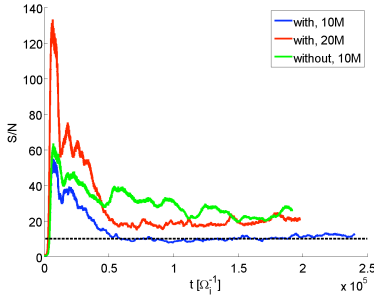## 5. Global nonlinear simulations of TEM turbulence

FIG. 8. Time evolution of the signal to noise ratio for the three TEM simulations. The horizontal dashed line indicates a SNR of 10
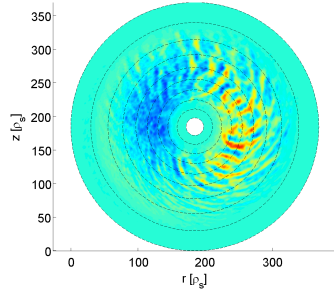
FIG. 9. Poloidal section of nonzonal component of the potential for the 10M simulation with the zonal flow included at $t=1.9 \cdot 10^5$ Ω_i^{-1}.
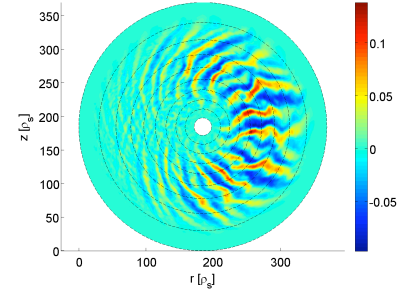
FIG. 10. Poloidal section of potential for the 10M simulation with the zonal flow artificially suppressed at $t=1.9 \cdot 10^5$ Ω_i^{-1}.

Very few works have been dealing with nonlinear TEM turbulence. However, flux-tube Eulerian simulations [15] showed that the zonal flow is subdominant at low and high density gradient. Flux-tube PIC simulations [14] showed that the zonal flow can have a stronger influence depending on the plasma parameters, but these simulations were done at a high density gradient value of $R_0/L_n=10$. ORB5 simulations have been run for CYCLONE parameters but with $\eta_i=1.0$ such that the dominant instability is an electron temperature gradient driven TEM. In order to reduce the simulation time, the mass ratio has been set to $m_e/m_i=0.01$, the simulation is run in annular mode between $s=0.1$ and $s=1.0$, and only the toroidal modes $\pm 4k$ have been solved, where k is an integer number, such that the number of

particles can be divided by 4 in comparison with a full torus simulation. A cut off has been applied for $k_\theta \rho_{Li} > 1.0$. Although the linear TEM spectrum extends to even shorter wavelength, the dominant toroidal modes in the nonlinear phase have $k_\theta \rho_{Li} \sim 0.3$. Three simulations have been performed: one with 10M ion and trapped electron markers, one with twice as many particles and one with 10M markers and the zonal flow artificially removed from the simulation. A 10M markers simulation takes $\sim 10^5$ CPU·hours on a BG/L machine.

Fig. 8 shows the SNR of these 3 simulations. The SNR for the 10M case with the zonal flow is probably too low. Figs. 9 and 10 show that the nonzonal component of the electric potential has more elongated structures when the zonal flow is dropped out of the simulation. When the zonal flow is included in the simulation, it dominates the other toroidal modes in amplitude and has an impact on heat transport: the heat diffusivity is higher (Fig. 11) but the temperature gradient is lower (Fig. 12). Although the initial burst is 2.5 times higher for the case without the zonal flow, the heat diffusivity slowly decreases to a level comparable to the case with the zonal flow included. The same behaviour can be observed for the normalized temperature gradient on Fig. 12. After the initial burst the electron temperature gradient drops but then the NCO slowly restores it back to the initial value. Note that the simulation should be run to
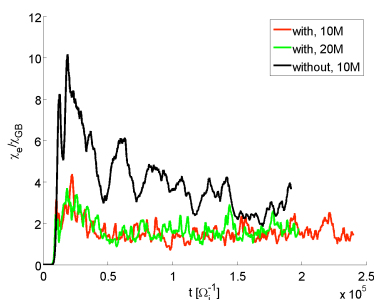

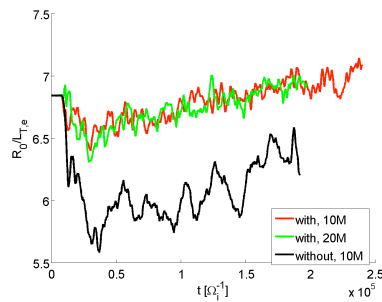FIG. 11. Time evolution of the electron heat diffusivity for the three TEM simulations.

FIG. 12. Time evolution of the normalized electron temperature gradient for the three TEM simulations.
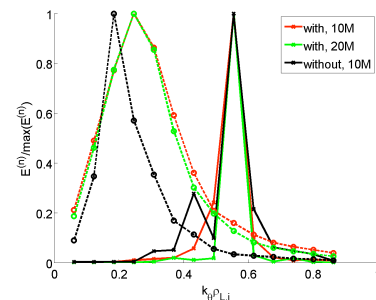
FIG. 13. Energy spectrum of the toroidal modes, normalized to the max. value in the linear phase (solid line, crosses) and in the late nonlinear phase, averaged between $t=10^5$ and $t=1.9\cdot10^5$ Ω_i^{-1} for the three TEM simulations.

even longer times to have constant low orders moments. Finally, Fig.13 plots the field energy spectrum of the toroidal modes in the linear and nonlinear phases. In the linear phase the spectra are strongly peaked, meaning that one toroidal mode strongly dominates. In the nonlinear phase, an energy cascade directed towards longer wavelengths ($k_\theta \rho_{Li} \sim 0.3$) is observed. The influence of the $k_\theta \rho_L$ cut-off on the TEM heat transport is still an open question and will be investigated in the future.

6. Conclusions

The noise control operator is an extremely powerful method to perform long and statistically converged simulations. As long as collisions are neglected, this work shows that this algorithm provides the necessary dissipation to reach a steady state, in decaying as well as in driven simulations. Simulations without the NCO reach a quasi-steady state for which the sum of the squared weights continuously increases, leading to intolerable noise levels. In this work it has been shown for the first time that numerical noise is responsible for the discrepancies

previously observed when the parallel nonlinearity was added or removed from the simulation. More generally, it means that one should carefully check the convergence of ITG PIC simulations. In the literature, much of the recent effort on numerical noise has been put on ETG simulations, where the undamped component of the perturbation plays a different role than in the ITG case. However the noise is also present in ITG simulations and can lead to premature conclusions. Further work is needed to gain more and more confidence in the gyrokinetic predictions.

Finally, this work shows the first ORB5 driven TEM simulations. Although the parameter space has not been explored yet, the first results indicate that, for the parameters considered, the zonal flow has some influence on the heat transport. In addition, a nonlinear cascade towards long wavelengths occurs. Future work will relax some of the approximations made in this work, like for example the filtering of toroidal modes, the mass ratio and the poloidal wavelength cutoff. The later is a crucial point for future gyrokinetic predictions. ITG, TEM and ETG turbulence are studied with appropriate scale separations for computational reasons. However, with the progresses of modern computers, simulations covering the spectrum from ion to electron wavelengths will become feasible. These huge simulations will be needed to validate *a posteriori* the scale separation approximation.

References

[1] W. M. Nevins *et al.*, Phys. Plasmas 12, 122305 (2005)
[2] Z. Lin *et al.*, Phys. Plasmas 12, 056125 (2005).
[3] F. Jenko *et al.*, Phys. Rev. Lett. 89, 225001 (2002).
[4] J. Krommes, Phys. Plasmas 6, 1477 (1999).
[5] Y. Chen *et al.*, Phys. Plasmas 4, 3591 (1997).
[6] B. F. McMillan *et al.*, Phys. Plasmas 15, 052308 (2008).
[7] S. Jolliet *et al.*, Comp. Phys. Commun. 177, 409 (2007).
[8] Z. Lin *et al.*, J. Phys. Conf. Ser. 16, 16 (2005).
[9] J. C. Kniep *et al.*, Comp. Phys. Commun. 164, 98 (2004).
[10] L. Villard *et al.*, Nucl. Fusion 44, 172 (2004).
[11] L. Villard *et al.*, Plasma Phys. Control. Fusion 46, B51 (2004).
[12] J. Candy *et al.*, Phys. Plasmas 13, 074501 (2006).
[13] Y. Idomura *et al.*, Journ. Comp. Phys., 226, 244 (2007).
[14] J. Lang *et al.*, Phys. Plasmas 14, 082315 (2007).
[15] T. Dannert *et al.*, Phys. Plasmas 12, 072309 (2005).
[16] T. S. Hamh, Phys. Fluids 31, 2670 (1988).
[17] A. Y. Aydemir, Phys. Plasmas 1, 822 (1994).
[18] P. Angelino *et al.*, Phys. Plasmas 13, 052304 (2006).
[19] M. Fivaz *et al.*, Comp. Phys. Commun 111, 27 (1998).
[20] J. Candy *et al.*, Phys. Plasmas 13, 032310 (2006).
[21] A. M. Dimits *et al.*, Phys. Plasmas 7, 969 (2000).
[22] A. Bottino *et al.*, Phys. Plasmas 14, 010701 (2007).
[23] R. Hatzky *et al.*, Phys. Plasmas 9, 898 (2002).
[24] Z, Lin *et al.*, Science 281, 1835 (1998).